A SIMPLE CONTROL LAW FOR REDUCING THE EFFECTIVE CHARACTERISTIC ACCELERATION OF A SOLAR SAIL

Matteo CERIOTTI[a,*], Gregory MAY-WILSON[a]

[a] *James Watt School of Engineering, University of Glasgow, Glasgow G12 8QQ, UK*

Abstract

The direction and magnitude of a solar sail acceleration are strongly related. For this reason, once the characteristic acceleration has been fixed, it is not possible to modulate the acceleration in a particular direction. In this work, a semi-analytical switching control law is derived, enabling a solar sail to emulate a smaller effective characteristic acceleration (without changes in geometry or optical properties); by periodically changing the pitch (cone) angle of the sail, in average over time, the acceleration produced by the sail matches exactly (in both direction and magnitude) that of a "smaller" sail. The range in which this is possible is determined, and the limitations on this range due to the size difference is computed. The method is validated on optimal Earth-Mars trajectories.

Keywords

Solar sail; control law; lightness number; characteristic acceleration; Optimal Earth-Mars trajectory.

Nomenclature

$\mathbf{a}$	Solar sail acceleration
a_c	Characteristic acceleration
a_{c0}	Characteristic acceleration of the "small" (emulated) sail
a_{cr}	Characteristic acceleration of the "large" (emulating) sail
A	Sail area
c	Speed of light
$\mathbf{f}_p$	Solar radiation pressure force vector
r_E	Sun-Earth distance (1 au)
r	Spacecraft distance from the sun
$\hat{\mathbf{u}}_i$	Incident radiation unit vector

[*] Corresponding author, matteo.ceriotti@glasgow.ac.uk

$\hat{\mathbf{n}}$ Sail normal unit vector

T_{switch} Switching period

W_E Solar energy flux at 1au

X,Y Constants

α Sail pitch (cone) angle

α_0 Emulated pitch angle

α_1, α_2 Emulating pitch angles

$\Delta\mathbf{r}_f$ Difference in final position

$\Delta\mathbf{v}_f$ Difference in final velocity

η Sail efficiency

θ Anomaly

σ Sail loading

Subscripts

f Final

r Radial component

r Referred to the “large” (emulating) sail

θ Transversal component

0 Referred to the “small” (emulated) sail

1. Introduction

One method to overcome the limitations of a reaction-mass propulsion system for spacecraft is the use of a solar sail (Vulpetti et al., 2015). A solar sail is a form of spacecraft propulsion for which the fuel is effectively unlimited, as the source of fuel is freely available in space, namely the light of the sun (Macdonald and McInnes, 2010).

A solar sail exploits solar radiation pressure: photons incident with an object will transfer momentum to that object, and likewise upon reflection will exert an additional force. The combination of transferred momentum and reflection produce a pressure force upon any surface upon which the photons interact, solar radiation pressure, and thus the object is accelerated by this pressure (Fu et al., 2016).

The potential Δv of the craft is effectively unlimited, this allows for significantly longer duration missions then would otherwise be available to a craft propelled by a reaction engine. Additionally, it allows for high energy missions requiring a large Δv, which would likewise be unrealistic for a spacecraft utilising a reaction engine as its source of propulsion.

The force generated by an ideal, perfectly-reflective solar sail is orientated normal to the surface of the sail membrane; this allows a solar sail to generate a force both along the velocity and against it, therefore producing an acceleration or deceleration of the spacecraft, depending on the cone (or pitch) angle, i.e. the angle of the sail normal to the incident photons (or the sun line).

The force due to solar radiation pressure scales in an inverse square ratio with the distance from the sun. However, the force due to sun gravity also has an inverse square relation to the radius from the sun, as a result at any distance from the sun the forces of gravity and solar radiation pressure are directly proportional. Because of this direct proportionality, a fixed-pitch-angle sail (with respect to the sun-sail line) will spiral outwards, or inwards, on a logarithmic spiral (McInnes and Cartmell, 2006).

Each photon carries a very small momentum; thus, a sail must be able to reflect a vast number of photons in order for the transferred momentum to impart a sensible acceleration, and shall be as near to a perfect mirror as possible to maximise the force.

A sail at an Earth orbit distance from the sun (1 au) will experience a solar radiation pressure of 9.08 μPa (Dalla Vedova et al., 2011). Sail materials must be incredibly light, a common construction of modern solar sails is a polymer sheet, in order to grant the sail flexibility and support, coated with a thin layer of aluminium, in order to provide as near perfect a reflector as possible, this construction allows the sail to have a low mass per unit area and a high reflectivity therefore allowing the sail to maximise its acceleration (McInnes, 1999).

The first interplanetary solar sail demonstrator was the Japanese IKAROS probe, launched on the 21st of May in 2010 (Tsuda et al., 2011). The intention of the IKAROS was to demonstrate solar sail technology in deep space flight (Funase et al., 2011). In 2019, the Planetary Society's LightSail 2 successfully raised its Earth orbit solely using solar radiation pressure (Nye, 2019).

An example of the requirements in size and mass for a solar sail can be seen in the cancelled Sunjammer spacecraft. Sunjammer was initially scheduled to be launched in January 2015 and was to be the largest ever solar sail with an area of 1,208 m^2 while weighing only 32 kg[1].

Due to the nature of the acceleration generated by a solar sail each sail will have an optimal trajectory for a given journey. As such, for a craft which is intended to make a complex mission, including multiple phases in different dynamical environment, sails of different (or varying sizes) may be desirable. This is however hard to achieve, due to mechanical limitations in the deployment mechanisms.

Potential applications are in the domain of asteroid missions, were a large-lightness sail is required for the Earth-to-asteroid transfer (interplanetary phase) (Peloni et al., 2016), while a small-lightness sail is desirable for motion near the asteroid's weak gravity field (Morrow et al., 2001); a large sail can easily produce an acceleration that is stronger than the asteroid's gravity (Moore and Ceriotti, 2019), therefore rendering orbiting around the asteroid impossible or extremely difficult to control (Zeng et al., 2016, Zeng et al., 2015).

The purpose of this work is to determine a control law for a large-characteristic-acceleration sail to produce, in average over an interval of time, the same acceleration of a solar sail with a smaller characteristic acceleration.

In particular, this work seeks to find a switching law between two pitch angles, such that the *average* acceleration of the two pitches is exactly equal to the acceleration of the emulated sail, in both magnitude and direction.

Once the control law is found, we will assume that such a sail will be able to navigate a trajectory designed for a smaller sail (and therefore "emulate" the smaller sail), and we will investigate the changes in the trajectory produced by using the larger sail with the new control law. This work will also show the limitations of this approach, in that not all sails can emulate each other, but conditions will be found in terms of pitch angle and ratio between characteristic accelerations.

2. Solar Sail Model

Considering, in the first approximation, a perfectly flat, perfectly reflective solar sail membrane, the force due to solar radiation pressure $\mathbf{f}_p$ acts along the sail normal, $\hat{\mathbf{n}}$, can be written as (McInnes and Brown, 1990):

[1] NASA, "Solar Sail Demonstrator ('Sunjammer')," URL: http://www.nasa.gov/mission_pages/tdm/solarsail/index.html [retrieved 15/02/2020].

$$\mathbf{f}_p = \frac{2AW_E\eta}{c}\left(\frac{r_E}{r}\right)^2 \left(\hat{\mathbf{u}}_i \cdot \hat{\mathbf{n}}\right)^2 \hat{\mathbf{n}} \tag{1}$$

where $\hat{\mathbf{u}}_i$ is the direction of the incident photons (or sun-to-sail line), r_E is the sun-Earth distance (1 au), r is the spacecraft distance from the sun, c is the speed of light, A is the sail area, W_E is the solar energy flux at the distance of 1 au, and η is an additional parameter representing the overall sail efficiency in terms of reflecting the photons. For a typical sail this value is within the range of 0.85 to 0.9, however for all studies within this paper a unitary value is assumed for sake of simplicity. Given the preliminary nature of this investigation, it is believed that this assumption is acceptable.

The sail loading σ is the mass of the spacecraft divided by the area of the reflecting surface:

$$\sigma = \frac{m}{A} \tag{2}$$

The dot product in Eq. (1) can also be expressed in term of cone or pitch angle α, which is the angle between $\hat{\mathbf{u}}_i, \hat{\mathbf{n}}$, i.e.:

$$\cos\alpha = \hat{\mathbf{u}}_i \cdot \hat{\mathbf{n}} \tag{3}$$

Combining (1), (2) and (3), an expression for the sail acceleration $\mathbf{a} = \mathbf{f}_p / m$:

$$\mathbf{a} = 2\frac{W_E\eta}{c}\frac{1}{\sigma}\left(\frac{r_E}{r}\right)^2 \cos\left(\alpha\right)^2 \hat{\mathbf{n}} \tag{4}$$

A universal metric for the performance of a solar sail (independent of the distance from the sun and pitch angle) is its characteristic acceleration (a_c), defined as the acceleration experienced by the sail when oriented such that the surface is normal to the sun line (a pitch angle $\alpha = 0$), and at a distance of 1 au from the sun (Wright, 1992). This can be expressed as a function of the sail loading and η only:

$$a_c = \frac{9.08\eta}{\sigma\left[\text{g m}^{-2}\right]}\left[\text{mm s}^{-2}\right] \tag{5}$$

where $2W_E/c \cong 9.08$ in the units indicated.

Typical characteristic accelerations observed in solar sails fall within a range of 0.1 mm s^{-2} to 0.5 mm s^{-2}, however future sails may have as high a characteristic acceleration as large as 2 mm s^{-2}.

By using Eq. (5), the sail acceleration in Eq. (4) can be expressed as a function of the characteristic acceleration, in place of the sail loading. In addition, as the acceleration experienced by a sail is directed along the sail normal, $\hat{\mathbf{n}}$, utilising the pitch angle α it is possible to decompose the total acceleration vector into the radial and transversal components:

$$\begin{aligned} a_r &= a_c \left(\frac{r_E}{r} \right)^2 \cos(\alpha)^3 \\ a_\theta &= a_c \left(\frac{r_E}{r} \right)^2 \cos^2(\alpha) \sin(\alpha) \end{aligned} \tag{6}$$

The envelope of acceleration of a solar can be calculated. Assuming a characteristic acceleration of 1 mm s^{-2} at a distance of 1 au from the sun, Fig. 1 shows this envelope of acceleration (blue curve) for a pitch angle $\alpha = [-90, 90]\text{deg}$. In radial and transversal components, the solar sail acceleration is ideally represented by an imaginary segment connecting the origin to a point along the envelope. This segment also represents the sail normal, and therefore the angle with the radial (vertical) axis is the pitch angle. Fig. 1 also shows, as an example, a red line representing the acceleration when the sail pitch is 30 deg.

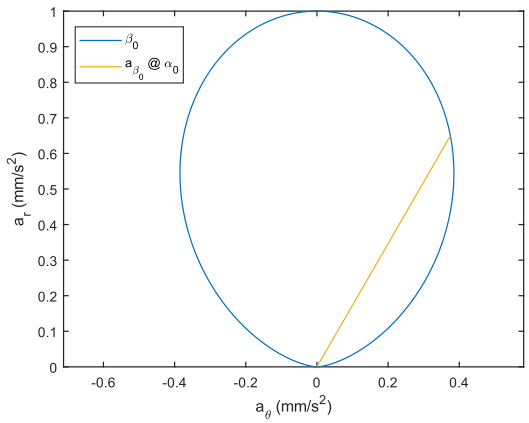

Fig. 1. Envelope of acceleration (in radial-transversal frame) for a sail with a characteristic acceleration of 1 mm s^{-2} in blue; the red line represents the acceleration vector of this sail at a pitch angle of 30 deg.

3. Acceleration and Pitch of the Large Sail

As can be seen from Eqs. (6), the acceleration of a solar sail is coupled in direction and magnitude. Varying the pitch angle α changes both magnitude and direction of the acceleration. In addition, the acceleration magnitude is directly proportional to the characteristic acceleration. However, the characteristic acceleration is mostly fixed by design, and can hardly be changed significantly (if at all) once the sail has deployed.

Let us consider now two sails of different characteristic accelerations, a_{c0} and a_{cr}, such that:

$$a_{c0} < a_{cr} \tag{7}$$

We will refer to the two sails as "small" and "large", with slight abuse of language as we are not referring to the actual size, but to the characteristic acceleration.

For what stated before, a sail with a_{cr} cannot instantaneously produce the same acceleration as a sail with smaller a_{c0} by simply changing the pitch angle.

However, in order for a sail to track a trajectory with a certain accuracy, it is only required that the acceleration is, over a certain interval of time, *in average* matching the planned one (both in radial and transversal directions). Trajectory tracking errors will be introduced in this process, and will depend on the frequency of the switching among other factors.

In this work, we will investigate a switching control law between two different pitch angles, α_1 and α_2. For simplicity, the switching will happen with a constant frequency, and therefore the sail spends the same interval of time at each of these two attitudes. The manoeuvring time between the two is neglected. In reality, this switch between pitch angles will have a duration, and thus affect the acceleration of the sail during the switch, effectively reducing the time spent at each pitch angle. The effects of the switch would therefore be greater at higher frequencies of oscillation due to the relative increase in time spent switching.

Under these assumptions, the average acceleration provided is:

$$\begin{aligned} a_r &= a_{cr}\left(\frac{r_E}{r}\right)^2 \frac{\cos^3(\alpha_1)+\cos^3(\alpha_2)}{2} \\ a_\theta &= a_{cr}\left(\frac{r_E}{r}\right)^2 \frac{\cos^2(\alpha_1)\sin(\alpha_1)+\cos^2(\alpha_2)\sin(\alpha_2)}{2} \end{aligned} \tag{8}$$

This acceleration, produced in average by the "large" sail of a_{cr}, shall equate that of the "small" sail of a_{c0}, in order to follow the same trajectory:

$$\begin{aligned} a_r &= a_{c0}\left(\frac{r_E}{r}\right)^2 \cos(\alpha_0)^3 \\ a_\theta &= a_{c0}\left(\frac{r_E}{r}\right)^2 \cos^2(\alpha_0)\sin(\alpha_0) \end{aligned} \tag{9}$$

By equating Eqs. (8) and (9), we obtain implicit expressions for the angles α_1 and α_2:

$$\begin{aligned} a_{cr}\left(\frac{r_E}{r}\right)^2 \frac{\cos^3(\alpha_1)+\cos^3(\alpha_2)}{2} &\equiv a_{c0}\left(\frac{r_E}{r}\right)^2 \cos^3(\alpha_0) \\ a_{cr}\left(\frac{r_E}{r}\right)^2 \frac{\cos^2(\alpha_1)\sin(\alpha_1)+\cos^2(\alpha_2)\sin(\alpha_2)}{2} &\equiv a_{c0}\left(\frac{r_E}{r}\right)^2 \cos^2(\alpha_0)\sin(\alpha_0) \end{aligned} \tag{10}$$

These equations can then be simplified: as the characteristic accelerations a_{c0}, a_{cr} of the solar sails are constant, and the pitch angle to be emulated α_0 is a pre-defined input value, these values can be combined in order to create two constants *X* and *Y*:

$$\begin{aligned} X(\alpha_0, a_{c0}/a_{cr}) &\triangleq \frac{2a_{c0}}{a_{cr}}\cos(\alpha_0)^3 \\ Y(\alpha_0, a_{c0}/a_{cr}) &\triangleq \frac{2a_{c0}}{a_{cr}}\cos(\alpha_0)^2\sin(\alpha_0) \end{aligned} \tag{11}$$

Rearranging:

$$\begin{aligned} \cos^3(\alpha_1)+\cos^3(\alpha_2) &= X \\ \cos^2(\alpha_1)\sin(\alpha_1)+\cos^2(\alpha_2)\sin(\alpha_2) &= Y \end{aligned} \tag{12}$$

Eqs. (12) can then be rearranged in order to find α_1 and α_2 thus allowing for a pair of equations which can be used to determine the pitch angles necessary for the "large" sail of a_{cr} to emulate (in average) the acceleration of the "smaller" sail of a_{c0}:

$$\begin{aligned} \alpha_1 &= \arctan\frac{Y-\cos^2(\alpha_2)\sin(\alpha_2)}{X-\cos^3(\alpha_2)} \\ \alpha_2 &= \arctan\frac{Y-\cos^2(\alpha_1)\sin(\alpha_1)}{X-\cos^3(\alpha_1)} \end{aligned} \tag{13}$$

Additionally, from Eqs. (11) it can be seen that the two necessary pitch angles are not dependent upon the individual characteristic accelerations, however they are dependent upon the ratio between the two characteristic accelerations, a_{cr}/a_{c0}. This ratio will be referred to as the characteristic acceleration ratio, and throughout this paper will be used to define the "larger" solar sail in relation to the "smaller" sail to be emulated.

With the equations necessary to determine the necessary pitch angles, an initial investigation into the variance of α_1 and α_2 was conducted. Fixed a value for the characteristic acceleration ratio, Eqs. (13) can then solved numerically, using a simple iterative method, such that the α_1 and α_2 values necessary for the larger sail to emulate this range of angles could be found. This investigation was repeated for multiple characteristic acceleration ratios such that any difference in necessary pitch angle between ratios could be determined.

To visualise this result, a "large" sail with a_{cr} = 1.25 mm s^{-2} is used; continuing the analysis in Fig. 1, the envelope of acceleration of this sail was then created and compared to that of the "smaller" sail of a_{c0} = 1 mm s^{-2}. Fig. 2 shows both envelopes. Additionally, the yellow segment represents the acceleration vector of the "smaller" sail at a pitch angle α_0, and the purple segments represent the acceleration vectors and pitch angles α_1 and α_2 of the "larger" sail necessary for it to average the acceleration of the smaller sail at α_0, as obtained through Eqs. (13); this results in (a) $\alpha_1 = -\alpha_2 = 21.82$ deg for α_0 = 0, (b) 0.59 deg and 40.37 deg respectively (a difference of 39.78 deg) for α_0 = 15 deg, (c) α_1 = 20.7 deg and α_2 = 52.86 deg, with a difference of 32.16 deg, for α_0 = 30 deg.

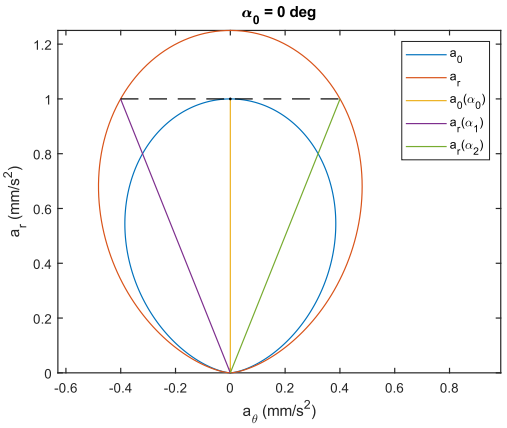

a)

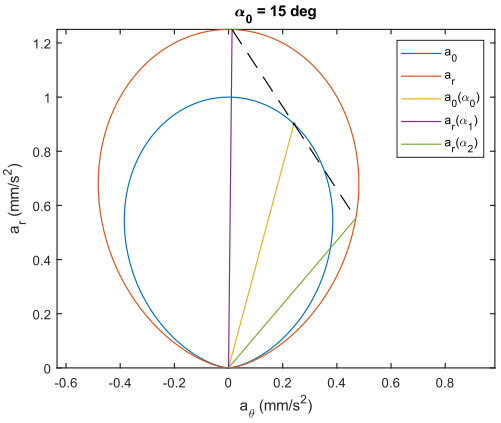

b)

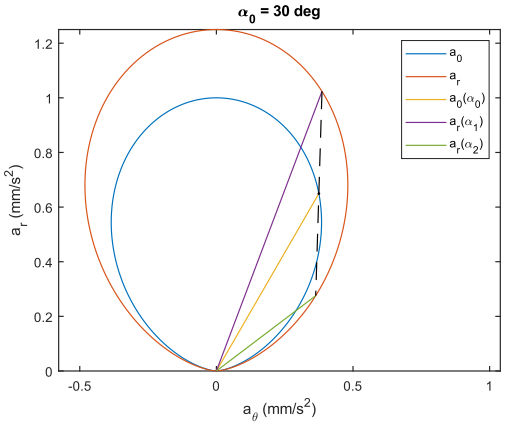

c)

Fig. 2. Envelopes of acceleration of a "small" sail of a_{c0} = 1 mm s^{-2} (blue), and a "large" sail of a_{cr} = 1.25 mm s^{-2} (red); the yellow segment represents the acceleration to be emulated; the purple segments represent the two accelerations and pitch angles of the larger sail that average out. a) α_0 = 0 deg; b) α_0= 15 deg; c) α_0= 30 deg.

3.1. α_1 and α_2 Values for α_0

Initially the values of the necessary pitch angles α_1 and α_2 were investigated and Eqs. (13) were used to calculate the necessary pitch angles α_1 and α_2 over the range of potential $\alpha_0 \in [0, 90]\text{deg}$, for specific characteristic acceleration ratios.

Fig. 3 shows the trend of the necessary pitch angles α_1 and α_2 with the angle to be emulated α_0 for two characteristic acceleration ratios.

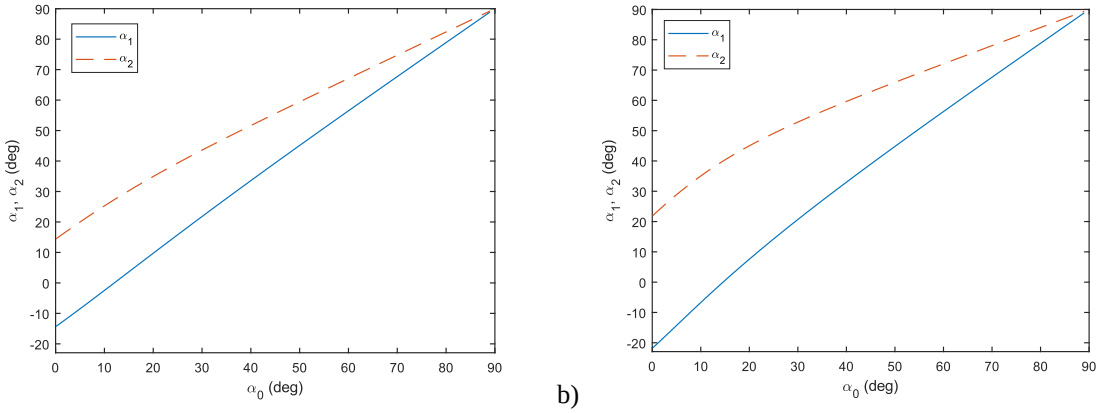

a) b)

Fig. 3. Values of necessary pitch angles α_1 and α_2 with emulated pitch angle α_0. a) characteristic acceleration ratio a_{cr}/a_{c0} = 1.1. b) a_{cr}/a_{c0} = 1.25.

Both figures show that the values of the necessary pitch angles increase with the angle to be emulated, however the difference between the two pitch angles reduces with the increase in α_0. It can also be seen that the increase is not linear (due to the non-linearity of Eqs. (13)): the larger of the two necessary pitch angles increases rapidly at low values of α_0 while at higher values of α_0 this rate of increase lowers.

An additional observation that can be made is that both pitch angles converge with α_0 at 90 deg. This result is expected as at this pitch angle there is no acceleration due to solar radiation pressure and so both α_1 and α_2 must also provide no acceleration in order to average the acceleration of the smaller sail when α_0 = 90 degrees.

It can also be noted through a comparison of the two figures that while the results from both characteristic acceleration ratios follow a similar trend the disparity between the α_1 and α_2 values determined for the larger characteristic acceleration ratio is greater than that for the smaller ratio at all values of α_0. In order to investigate this disparity, the variance of α_1 and α_2 for a third larger characteristic acceleration ratio of 1.4 was determined.

Fig. 4 shows the trend of α_1 and α_2 over the full range of $\alpha_0 \in [0, 90]\text{deg}$, for a higher characteristic acceleration ratio a_{cr}/a_{c0} = 1.4. It can be seen that above a certain value of α_0 there are no more feasible values of α_1 and α_2. It can therefore be concluded that large characteristic acceleration ratios place an (upper) limit upon the range of α_0 values for which there are potential solutions for α_1 and α_2.

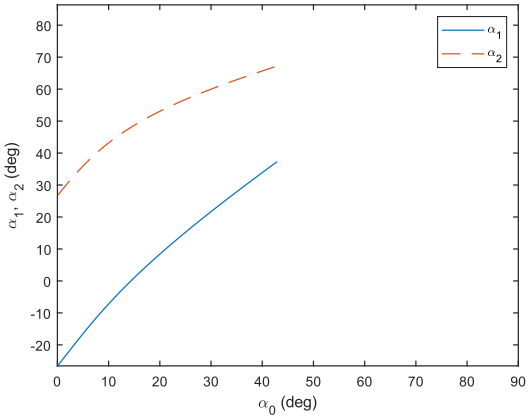

Fig. 4. Variance of necessary pitch angles α_1 and α_2 with emulated pitch angle α_0 for a sail with a characteristic acceleration ratio a_{cr}/a_{c0} = 1.4, the cut off at which there are no more viable solutions for α_1 and α_2 can be seen.

3.2. Limits due to Characteristic Acceleration ratio

In order to determine the extent of this limit, an investigation into the maximum α_0 value at which there are solutions for α_1 and α_2 for a range of characteristic acceleration ratios was conducted. Fig. 5 shows a plot of the maximum value of α_0 at which there are solutions for α_1 and α_2 over a range of characteristic acceleration ratios.

It can be seen from Fig. 5 that below a characteristic acceleration ratio of about 1.3 there are no limitations upon the range of α_0 values that produce viable results of α_1 and α_2 (all pitch angles can be emulated). However, above this value, the maximum α_0 that produces viable solutions for α_1 and α_2 rapidly decreases, and this rate of decrease declines as the characteristic acceleration ratio increases. However, as this ratio approaches a value of 2, the maximum α_0 value again decreases more rapidly. It was found that at a characteristic acceleration ratio of 2, the only viable solution was at a pitch angle α_0 of 0 deg, and above a characteristic acceleration ratio of 2 there were no more solutions for α_1 and α_2 at any value of α_0.

To fully appreciate the behaviour of the emulating pitch angles, Fig. 6 shows α_1 and α_2 as surfaces, functions of acceleration ratio and α_0. It appears again that the surfaces do not cover the entire domain, leaving out the area defined by the maximum emulated pitch angle in Fig. 5.

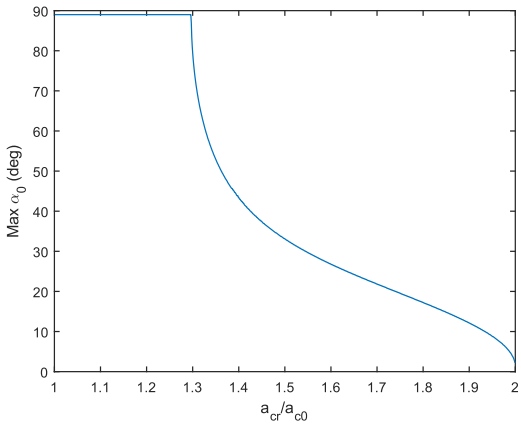

Fig. 5. Maximum pitch angle α_0 at which there are available solutions for α_1 and α_2 as a function of the characteristic acceleration ratio a_{cr}/a_{c0}.

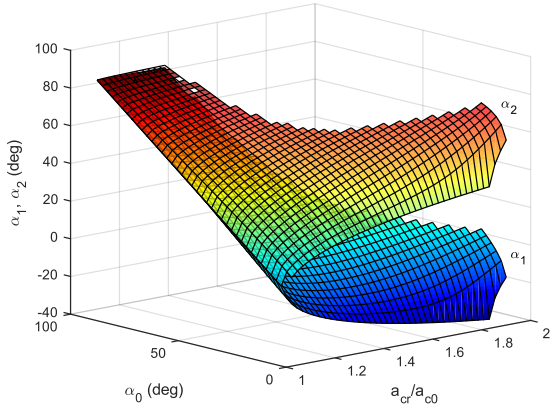

Fig. 6. Surfaces defined by the switching angles α_1 and α_2 as functions of acceleration ratio a_{cr}/a_{c0} and emulated pitch angle α_0.

4. Spiral Trajectory and Sensitivity Analysis

As Secs. 3.1-3.2 have shown that it is possible for a larger sail to average the acceleration of a smaller sail through oscillation of the pitch angle, an investigation was conducted into whether this could be applied to a real trajectory (Van Der Ha and Modi, 1979).

Initially, a simple spiral trajectory utilising a fixed pitch angle was chosen to be emulated. The sail starts its interplanetary journey at the Earth with zero excess velocity. A characteristic acceleration of 1 mm s^{-2} was chosen for the smaller sail, the 10-year trajectory followed by this sail with a fixed pitch angle of 30 deg was then computed, and the final position and velocity recorded, see Table 1. Trajectories are numerically integrated with MATLAB's *ode45* with absolute and relative tolerance of 10^{-8}.

Table 1. Initial and (reference) final position and velocity of the sail after a 10-year spiral trajectory.

	Initial	Final
Radius, r, km	1.496×10^{8}	1.11×10^{9}
Anomaly, θ, deg	0	246.75
Radial velocity, v_r, km/s	0	0.875
Transversal velocity, v_θ, km/s	29.979	8.737

With these determined values, the same trajectory was then emulated using a larger sail. A sail with a characteristic acceleration 1.25 mm s^{-2} was chosen, which guarantees that the full range of pitch angles are available.

Fig. 7 shows the nominal spiral trajectory followed by the sail with a_{c0} = 1 mm s^{-2} and the trajectory of the sail with a characteristic acceleration ratio of 1.25 emulating this trajectory. We selected two reference values for period of oscillation between pitch angles: 0.01% of the total time of flight (equivalent to 8.766 h), and 2% (73 d). Table 2 shows numerically the final state and error for these two cases. It can be noted that at the lower period, there is a marginal difference between the two trajectories; instead, the trajectory and final state are substantially different at the higher period (the most affected being the radial velocity). The next sections will quantify the error varying some of the parameters within these limits.

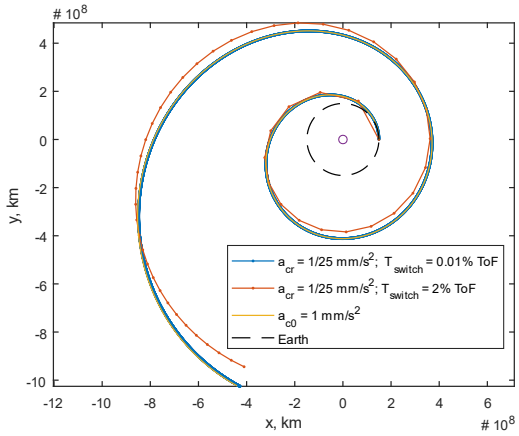

Fig. 7. 10-year spiral trajectory at a fixed pitch angle of 30 deg with a_{c0} = 1 mm s^{-2}, and trajectories emulated using a_{cr} = 1.25 mm s^{-2} and a switching period of 8.766 h (0.01% of time of flight) and 73 d (2%). The markers are at the sail switching.

Table 2. Final positions and velocities of the emulated trajectories, and errors with respect to the reference (Table 1).

	T_{switch} = 8.766 h (0.01%)			T_{switch} = 73 d (2%)		
	Final	Error		Final	Error	
		Absolute	%		Absolute	%
Radius, r, km	1.11×10^{9}	-3.150×10^{6}	-0.28%	1.03×10^{9}	-8.45×10^{7}	-7.59%
Anomaly, θ, deg	246.75	0.011	*n/a*	246.50	-0.042	*n/a*
Radial velocity, v_r, km/s	0.875	-0.009	-1.01%	0.185	-0.689	-78.8%
Transversal velocity, v_θ, km/s	8.737	0.028	0.31%	9.479	0.743	8.5%

4.1. Effect of the Frequency of Switching

The effect of the frequency of switching on the error in position and velocity of the solar sail at the final point are now investigated. The same spiral trajectory and sails in Sec. 4 are used. The final position and velocity of the sail were recorded over a range of periods of switching, and the error relative to the final position and velocity of the smaller sail on the trajectory intended to be emulated computed.

The effects of different periods of oscillation on the nominal trajectory that was computed in Sec. 4 were then calculated. A range of periods peaking at 73.05 h, 2% of the total flight time, were investigated, and the differences at the final time of flight in position and velocity, $\|\Delta\mathbf{r}_f\|, \|\Delta\mathbf{v}_f\|$ respectively, were noted.

Fig. 8 shows the differences in position and velocity on this trajectory (with respect to the reference trajectory of the "small" sail of a_{cr} = 1 mm s^{-2}) when larger sails of characteristic acceleration a_{cr} = 1.1, 1.25, 1.4 mm s^{-2} were used for emulation.

As expected, larger periods of oscillation produce larger errors in position and velocity at the final time. It is interesting to note that the smallest sail of the three does not always produce the smallest errors, while the largest sail produces small errors in final velocity but large in position.

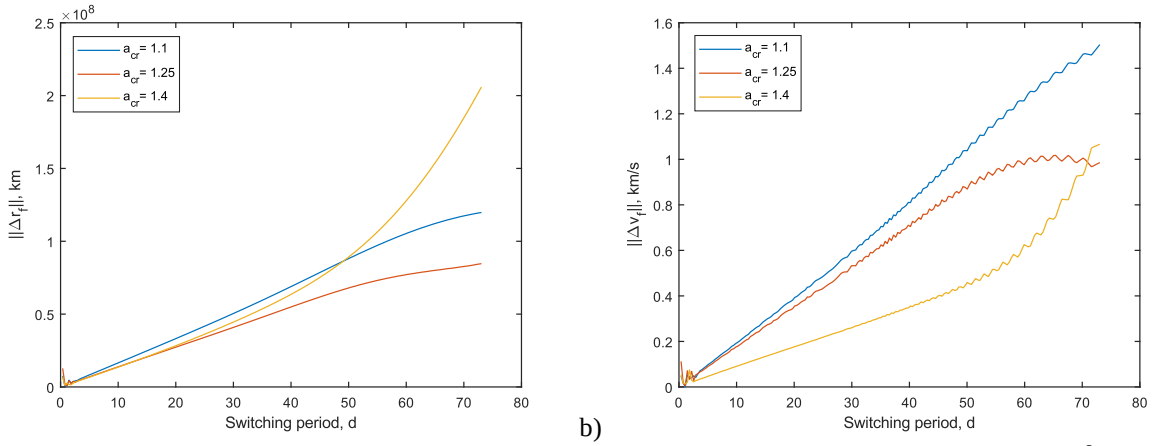

a) b)

Fig. 8. Errors in final position and velocity against the period of oscillation for a sail of a_{cr} = 1.1, 1.25, 1.4 mm s^{-2}, emulating one of a_{c0}= 1 mm s^{-2}.

4.2. Effect of Characteristic Acceleration Ratio

Similarly to the previous section, an investigation into the effect of changing the characteristic acceleration ratio at specific periods of oscillation is conducted. Three periods of switching were selected, namely 3.65 h, 36.52 h and 73 h, corresponding to 0.1%, 1% and 2% of the total flight time, respectively. Due to limitations upon the available solutions of α_1 and α_2, as seen from Fig. 5, the characteristic acceleration ratio was upper limited to 1.5, as higher values would provide no viable results for this trajectory in which $\alpha_0 = 30\ \text{deg}$.

Fig. 9 shows the sensitivity of the final position and velocity varying the characteristic acceleration of the "large" sail, for three different values of the switching period. Confirming the previous results, a higher switching period is always reflected in a larger final error (both in position and velocity). However, and interestingly, the same cannot be said for the characteristic acceleration: the error increase is not linear nor monotonous; while the error is very small for all characteristic accelerations in the range at small switching periods (blue lines), for larger switching periods, the error rapidly increases initially, for then decreasing again into a local minimum, for then increasing again. The characteristic acceleration of the large sail corresponding to this second minimum varies depending on the switching time, as can be seen following the red and yellow lines in both Fig. 9a and Fig. 9b. We can then infer that, in a hypothetical scenario of mission design, there is an optimal characteristic acceleration to emulate a smaller sail (apart from the trivial $a_{c0} \equiv a_{cr}$), which minimises the final error. We also note that unfortunately the point of minimum error in position does not match the point of minimum error in velocity, hence a compromise is to be made.

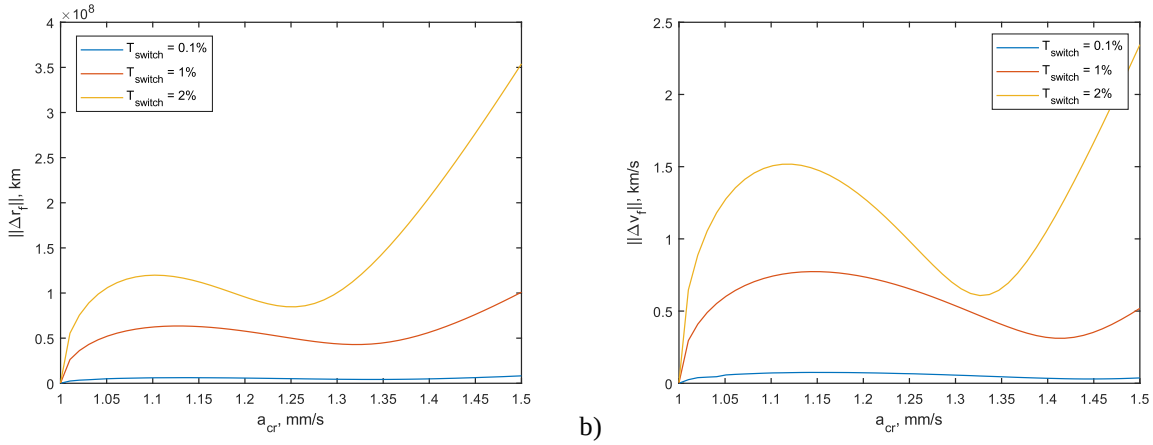

Fig. 9. Errors in final position and velocity against the characteristic acceleration ratio of the sail (emulating a_{c0}= 1 mm s^{-2}) at three distinct periods of oscillation.

4.3. Combined Errors due to Characteristic Acceleration Ratio and Switching Period

As previous analyses in Secs. 4.2 and 4.3 have shown, both characteristic acceleration ratio and frequency of oscillation influence the trajectory errors. To conclude this sensitivity analysis, we present the final errors when both parameters are varied at the same time. Fig. 10 shows the combined absolute error in position (a, b) and velocity (c, d), respectively, over a range of both periods of oscillation and characteristic acceleration ratios. The plots essentially give a qualitative and quantitative overview of the sensitivity of the trajectory to the parameters. As mentioned before, the locus of local minima can be identified in terms of characteristic acceleration ratio. It is also visible that the error ramps up relatively quickly as soon as the characteristic acceleration ratio increases (before decreasing again), while it increases comparatively slowly with the period of switching (but monotonically in average, except for some noise).

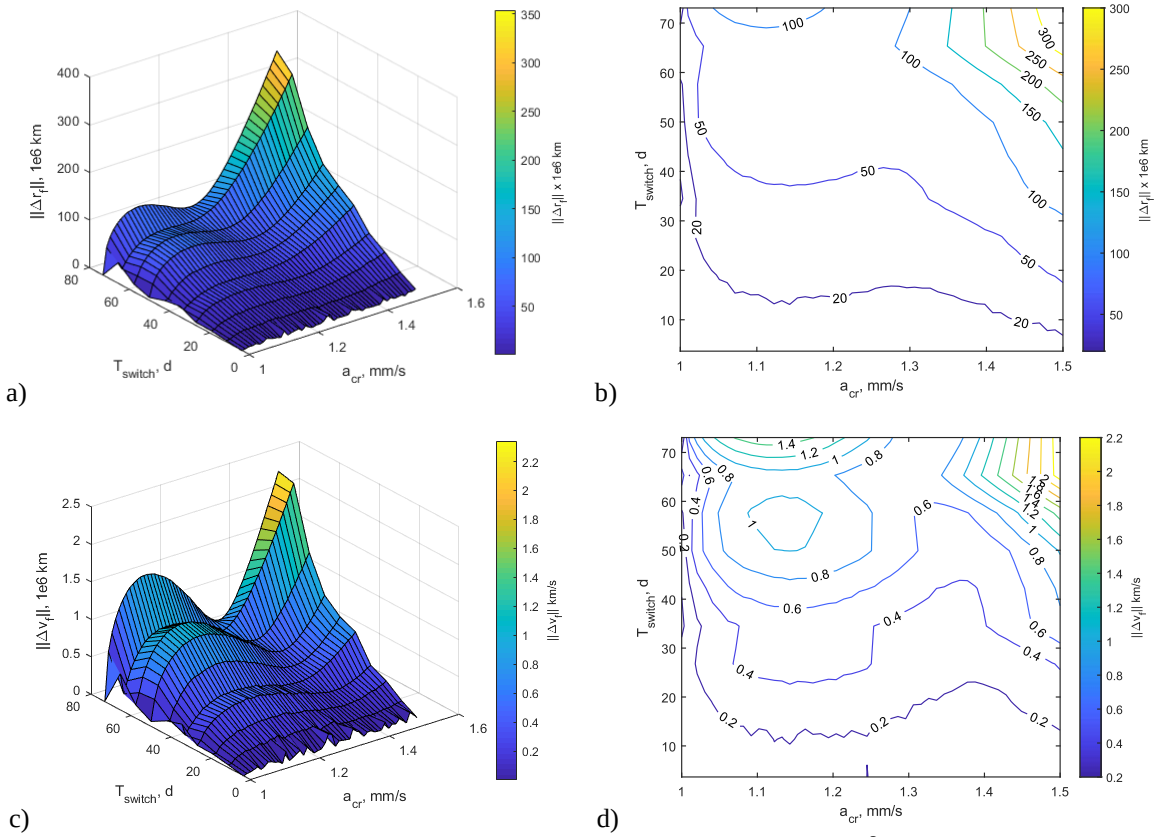

Fig. 10. Absolute errors in against characteristic acceleration ratio (with a_{c0}= 1 mm s^{-2}) and period of oscillation. a), b) Position; c),d) Velocity.

4.4. Effect of finite manoeuvring time

In the model used so far, it has been assumed that the sail instantaneously switches between the two emulating pitch angles α_1 and α_2, effectively neglecting the manoeuvring time. This justifies the results in Sec. 4.1, where a low period of oscillation (high frequency) produces very small trajectory errors. In reality, the sail will require a finite amount of time to slew from α_1 and α_2, and during this time, a variable acceleration is produced. Assuming a rest-to-rest manoeuvre with constant angular velocity, the average acceleration $\langle \mathbf{a} \rangle$ provided by the sail, during a slew manoeuvre from α_1 and α_2, is:

$$\langle a_r \rangle = \frac{\int_{\alpha_1}^{\alpha_2} a_r(\alpha) d\alpha}{\alpha_2 - \alpha_1}$$

$$\langle a_\theta \rangle = \frac{\int_{\alpha_1}^{\alpha_2} a_\theta(\alpha) d\alpha}{\alpha_2 - \alpha_1}$$

where the expressions for the acceleration are in Eq. (6). Fig. 11 shows the accelerations for the same parameters as in Fig. 2(b), i.e. a_{c0} = 1 mm s^{-2}, a_{cr} = 1.25 mm s^{-2}, α_0 = 15 deg; in addition, the average acceleration vector during the manoeuvre has been plotted (dotted line), together with the envelope generated by such vector over all values of α_0. It results that, for the emulated pitch angle in question of 15 deg, the average acceleration during the manoeuvre exceeds the emulated one both in radial and transversal components. While not shown here, the same happens for a wide range of emulated pitches around the origin.

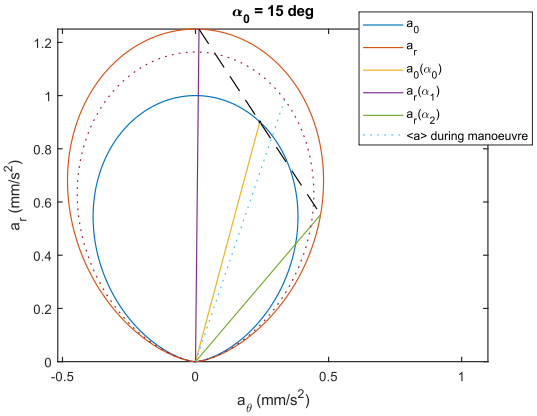

Fig. 11. Same case as in Fig. 2(b), additionally showing the average acceleration vector (dotted line) during a constant-speed manoeuvre from α_1 to α_2. The dotted curve is the envelope of average acceleration vectors for all values of α_0.

We can therefore conclude that the manoeuvring interval contributes with an acceleration that does not match the emulated one, affecting the trajectory navigation, and therefore this time shall be reduced to the minimum for the best emulation of the nominal trajectory. In addition, this negative effect will be even more significant for low periods of oscillation, because the slew manoeuvre needs be repeated more frequently over time.

Therefore, the mission designer is faced with a trade-off, where the lowest switching time is desirable on one side (to average the acceleration of the emulating pitches), but on the other side it should not be too small because of the finite manoeuvring time (or too much time will be spent manoeuvring). It is expected that there exist an "optimal frequency", which will depend on the emulating pitch angle, the characteristic acceleration ratio, the maximum slew rate of the sail, and the nominal trajectory itself. Because of the number of variables involved, we deem this analysis too specific for the scope of this paper.

5. Optimal Earth-to-Mars Trajectories

With the effects of oscillation upon a trajectory utilising a fixed α_0, an optimal Earth-to-Mars trajectory was chosen to be emulated. The Earth and Mars orbits are approximated as circular for simplicity. The optimal (minimum time) control history of the pitch angle for two different nominal characteristic accelerations, a_{c0}= 0.1 and 1 mm s^{-2}, were calculated using the method by Sullo et al. (2017).

For the smaller value of characteristic acceleration, it is found that for the initial stage of this trajectory, the sail spirals in towards the sun, using a negative pitch angle for a relatively short duration before returning to a positive pitch angle in order to spiral outwards (see dotted blue lines in Fig. 12a and Fig. 13a, named "reference"). Due to this,, the pitch angle α_0 switches from -90 deg to +90 deg, as can be seen in Fig. 12b and Fig. 13b, at roughly 332 d into the time of flight (blue line, named α_0). Therefore, according to the limitations determined in Sec. 3.1 a characteristic acceleration ratio below 1.3 must be selected in order for all the pitch angles α_0 to produce viable solutions of α_1 and α_2, in this case a ratio of 1.25 was selected (resulting in a_{cr}= 0.125 mm s^{-2}).

The time histories for the necessary α_1 and α_2 values were calculated (see red and yellow lines in Fig. 12b and Fig. 13b, named α_{r1} and α_{r2}), and the trajectory of the larger sails were then integrated with the new control law.

The switching control law is also plotted in Fig. 12b and Fig. 13b (dotted purple line named α, switching between the two control angles α_1 and α_2), for two different periods of switching, 6 months and 1 month, respectively.

The emulated trajectories are shown in Fig. 12a and Fig. 13a, in solid black line, for the two switching periods.

Table 3 quantifies the final errors in the emulated trajectory, with respect to the reference, for both switching periods. The errors are shown in terms of position and velocity, in polar coordinates and radial/transversal components. The error percentages (%) are computed on the magnitude of the position and velocity vectors, respectively.

Starting from the case T_{switch} = 6 months (Fig. 12a), it is notable how the general trend of the trajectory is similar to the reference, even with such a long switching period. However, the emulated trajectory quickly diverges from the reference, and the final point is therefore considerably far. Instead, reducing the switching time to T_{switch} = 1 month, vastly improves the accuracy of the emulated trajectory, at the point that it becomes indistinguishable from the reference in the orbit plot. These qualitative results are confirmed numerically with the error values in Table 3: both position and velocity component errors are below 0.1% of their magnitude, and the true anomaly is within 3 deg. It is likely that these small errors can be easily corrected with a simple optimisation procedure.

Of course, lower errors come with the trade-off of additional (and more frequent) control required by the emulating sail. A full mission analysis would assess the trade-off between sail switching and allowed errors on the final states.

In the case of a_{c0} = 1 mm s^{-2}, the range in pitch angle α_0 along the optimal, reference trajectory was considerably smaller, allowing for a greater range of characteristic acceleration ratio to be available; however, in order to be consistent with the previous case, a ratio of 1.25 was also chosen for this case (resulting in a_{cr}= 1.25). Analogously to the previous example, the reference control and trajectory are plotted in Fig. 14 and Fig. 15: given the higher characteristic acceleration, the time of flight is considerably shorter, taking 429 days to reach Mars' orbit. Therefore, we considered two switching periods of 1 month and 20 days for this scenario, respectively.

Emulated trajectories are plotted in Fig. 14a and Fig. 15a, and errors on final states are quantified in Table 4. In this case, it is interesting to note that a relatively small reduction in switching period (1/3 less) results in a reduction in the final error by one order of magnitude, from around 3% and 10 deg in anomaly, to around 0.5% and less than 2.5 deg.

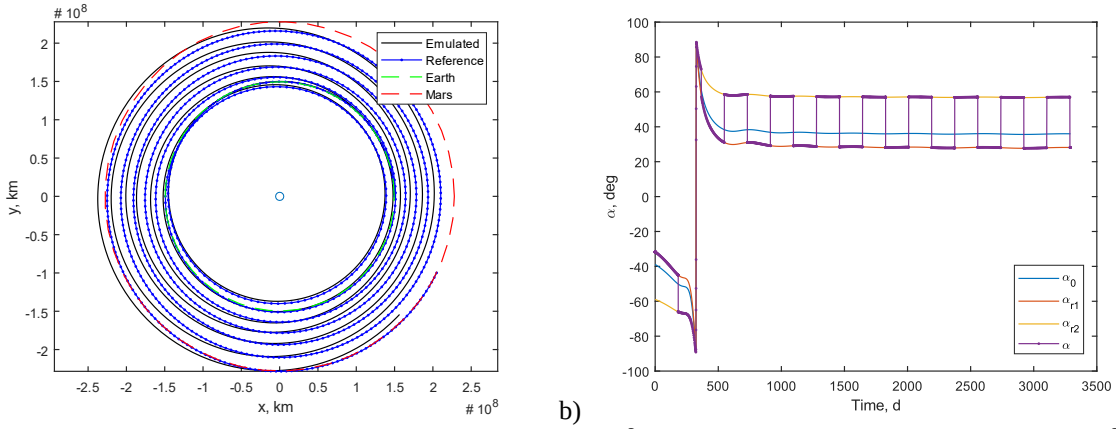

a) b)

Fig. 12. Optimal Earth-Mars transfer for a sail with a_{c0} = 0.1 mm s^{-2} and emulated by a sail with a_{cr} = 0.125 mm s^{-2} (ratio 1.25), T_{switch} = 6 months. a) Nominal optimal trajectory with a_{c0} = 0.1 mm s^{-2} and emulated with a_{cr} = 0.125 mm s^{-2}. b) Time histories of pitch angles α_0, α_1 and α_2, with the switching control law highlighted.

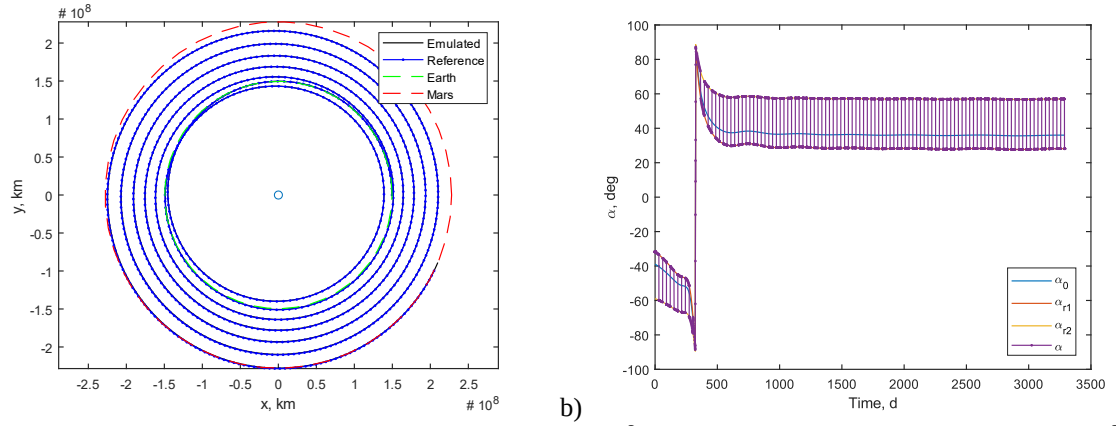

a) b)

Fig. 13. Optimal Earth-Mars transfer for a sail with a_{c0} = 0.1 mm s^{-2} and emulated by a sail with a_{cr} = 0.125 mm s^{-2} (ratio 1.25), T_{switch} = 1 month. a) Nominal optimal trajectory with a_{c0} = 0.1 mm s^{-2} and emulated with a_{cr} = 0.125 mm s^{-2}. b) Time histories of pitch angles α_0, α_1 and α_2, with the switching control law highlighted.

Table 3. Errors in final state for the optimal Earth-to-Mars trajectories with a_{c0} = 0.1 mm/s^2.

	T_{switch} = 6 months		T_{switch} = 1 month	
	Absolute	%	Absolute	%
Δr , km	8.25×10^6	3.6	8.26×10^4	0.03
$\Delta\theta$, deg	18.6	*n/a*	3.01	*n/a*
Δv_r , km/s	0.683	2.8	0.05	< 0.01
Δv_θ , km/s	0.922	3.8	< 0.01	0.02

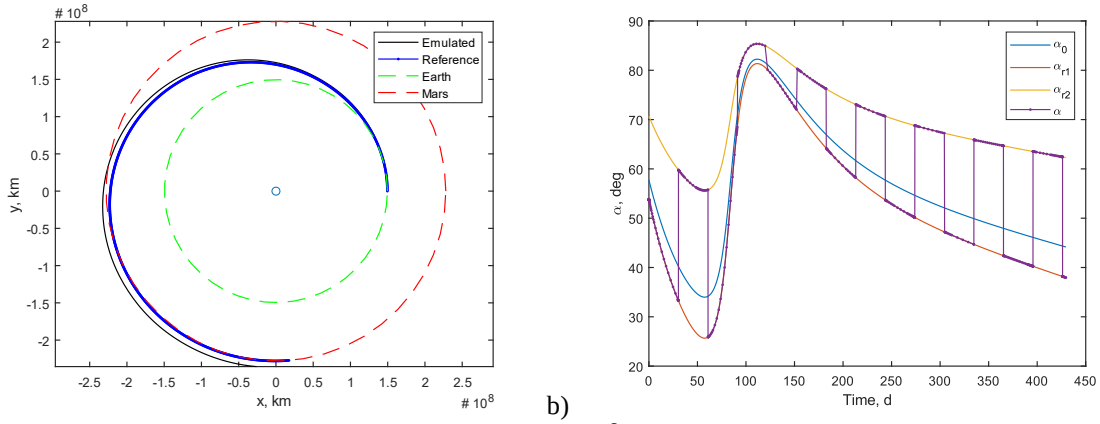

a) b)

Fig. 14. Optimal Earth-Mars transfer for a sail with a_{c0} = 1 mm s^{-2} and emulated by a sail with a_{cr} = 0.125 mm s^{-2} (ratio 1.25), T_{switch} = 1 month. a) Nominal optimal trajectory with a_{c0} = 0.1 mm s^{-2} and emulated with a_{cr} = 0.125 mm s^{-2}. b) Time histories of pitch angles α_0, α_1 and α_2, with the switching control law highlighted.

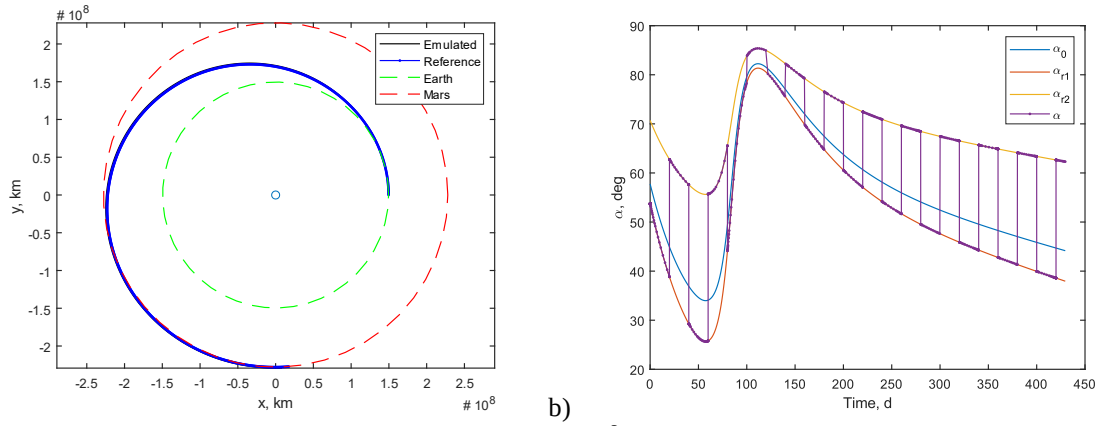

a) b)

Fig. 15. Optimal Earth-Mars transfer for a sail with a_{c0} = 1 mm s^{-2} and emulated by a sail with a_{cr} = 0.125 mm s^{-2} (ratio 1.25), T_{switch} = 20 days. a) Nominal optimal trajectory with a_{c0} = 0.1 mm s^{-2} and emulated with a_{cr} = 0.125 mm s^{-2}. b) Time histories of pitch angles α_0, α_1 and α_2, with the switching control law highlighted.

Table 4. Errors in final state for the optimal Earth-to-Mars trajectories with a_{c0} = 1 mm/s^2.

	T_{switch} = 1 month		T_{switch} = 20 days	
	Absolute	%	Absolute	%
Δr , km	9.06×10^6	3.97	1.31×10^6	0.57
$\Delta\theta$, deg	10.7	*n/a*	2.29	*n/a*
Δv_r , km/s	0.54	2.22	0.03	0.12
Δv_θ , km/s	0.88	3.65	0.09	0.38

6. Conclusions

The aim of this project was to determine a control law for which a “large” solar sail could produce, in average over some time, the same acceleration of a “smaller” sail, in magnitude and direction, through a control law periodically switching between two pitch angles. It was shown that such control law exists, and the pitch angles were derived. However, it was found that there is an upper limit on the pitch angle that can be emulated, and this limit is function of the characteristic acceleration ratio between the “large” and the “small” sail. Specifically, as the characteristic acceleration ratio increases, the upper limit on the pitch angle decreases.

The switching control law was implemented and tested on a simple heliocentric spiral trajectory. The “small” sail followed a nominal control law with constant pitch angle. It was found that the errors produced using the “large” sail through the switching law increase as the switching period increases, as well as the characteristic acceleration ratio.

Finally, the emulation was tested on two optimal Earth-to-Mars solar sail trajectories, with two different characteristic accelerations and switching periods. It was shown that, by selecting an appropriate switching period, the errors at Mars can be essentially neglected, and that a small reduction of the switching period can have a large effect in reducing these errors.

The characteristic acceleration ratio of 1.25 also allows to emulate all pitch angles, therefore can be used for any arbitrary control law. It can therefore be concluded that this switching control law between pitch angles is not limited to simple trajectories, and could be applied to more complex transfers and sail control problems.

6.1. Future Work

The authors envisage the following future research steps.

6.1.1. Finite-Time Steering Manoeuvres

Throughout this paper the assumption was made that the switch from one pitch angle to the other was effectively instantaneous, in reality this would have a finite duration. During the duration of the switch the acceleration due to solar radiation pressure acting upon the sail would obviously be affected and, as such, the average acceleration experienced by the solar sail would differ from the value that was calculated for an instantaneous change. As such, further research will derive an emulating control law that aims at replicating the sail acceleration in average, considering finite-time steering manoeuvres.

6.1.2. Non-Periodic Switches

This work assumed that the switching was between two pitch angles, and with a periodic time-law. However, a wider range of emulation could be achieved if one is to consider a switching law between two angles, with a different stay time in each one.

6.1.3. 3D Manoeuvres

One can also envisage switching not just between two angles, but among three or more angles cyclically, to achieve the desired average acceleration. There might be more than one solution to the problem, in which case the best solution (according to some metric) could be selected.

Finally, the current method uses switches in the pitch angle, meaning that the clock angle (the angle identifying the rotation of the sail normal around the sun line) is kept constant. However, in reality, more efficient strategies could be found if not only the pitch, but also the clock angle were to be changed simultaneously.

6.1.4. Application to more complex trajectories

We have proven numerically that the proposed control law is suitable for interplanetary, heliocentric transfers; following investigations shall be done on more complex trajectories, such as periodic orbits in the three-body problem and orbits around small bodies such as asteroids.

Acknowledgements

Matteo Ceriotti would like to thank the James Watt School of Engineering (University of Glasgow) and the Institution of Mechanical Engineers (IMechE Conference Grant EAC/KDF/OFFER/19/046) for supporting part of this work.

The authors thank two anonymous reviewers for constructive comments which improved the work, and in particular one who provided interesting insights on the effects of finite manoeuvring time, which are discussed in Sec. 4.4.

References

Dalla Vedova, F., Henrion, H., Leipold, M., et al. The Solar Sail Materials (SSM) project – Status of activities. Advances in Space Research 48 (11), 1922-1926, doi: 10.1016/j.asr.2011.08.003, 2011.

Fu, B., Sperber, E., Eke, F. Solar sail technology—A state of the art review. Progress in Aerospace Sciences 86 (Supplement C), 1-19, doi: 10.1016/j.paerosci.2016.07.001, 2016.

Funase, R., Shirasawa, Y., Mimasu, Y., et al. On-orbit verification of fuel-free attitude control system for spinning solar sail utilizing solar radiation pressure. Advances in Space Research (Special issue Solar Sailing) 48 (11), 1740-1746, doi: 10.1016/j.asr.2011.02.022, 2011.

Macdonald, M., McInnes, C.R. Solar sail mission applications and future advancement. *2nd International Symposium on Solar Sailing (ISSS 2010)*, edited by Kezerashvili, R.Y., New York, NY, USA, pp. 7-26, 2010.

McInnes, C.R. Solar sailing: technology, dynamics and mission applications. Springer-Verlag, Berlin, 1999.

McInnes, C.R., Brown, J.C. Solar sail dynamics with an extended source of radiation pressure. Acta Astronautica 22, 155-160, doi: 10.1016/0094-5765(90)90017-F, 1990.

McInnes, C.R., Cartmell, M.P. Orbital Mechanics of Propellantless Propulsion Systems. In: Gurfil, P., (Ed.). Elsevier Astrodynamics Series. Butterworth-Heinemann, pp. 189-235, 2006.

Moore, I., Ceriotti, M. Solar sails for perturbation relief: application to asteroid proximity operations. *5th International Symposium on Solar Sailing (ISSS 2019)*, Aachen, Germany, 2019.

Morrow, E., Scheeres, D.J., Lubin, D. Solar sail orbit operations at asteroids. Journal of Spacecraft and Rockets 38 (2), 279-286, doi: 10.2514/2.3682, 2001.

Nye, B. Mission Success! LightSail 2 demonstrates flight by light. The Planetary Report. The Planetary Society, pp. 4-5, 2019.

Peloni, A., Ceriotti, M., Dachwald, B. Solar sail trajectory design for a multiple near-Earth asteroid rendezvous mission. J Guid Control Dynam 39 (12), 2712-2724, doi: 10.2514/1.G000470, 2016.

Sullo, N., Peloni, A., Ceriotti, M. Low-thrust to solar-sail trajectories: a homotopic approach. J Guid Control Dynam 40 (11), 2796-2806, doi: 10.2514/1.G002552, 2017.

Tsuda, Y., Mori, O., Funase, R., et al. Flight status of IKAROS deep space solar sail demonstrator. Acta Astronautica 69, 833-840, doi: 10.1016/j.actaastro.2011.06.005, 2011.

Van Der Ha, J.C., Modi, V.J. Long-term evaluation of three-dimensional heliocentric solar sail trajectories with arbitrary fixed sail setting. Celestial mechanics 19 (2), 113-138, doi: 10.1007/bf01796085, 1979.

Vulpetti, G., Johnson, L., Matloff, G.L. Solar Sails - A novel approach to interplanetary travel. Springer, New York, NY, USA, 2015.

Wright, J.L. Space sailing. Gordon and Breach, Philadelphia, PA (USA), 1992.

Zeng, X.Y., Gong, S.P., Li, J.F., et al. Solar Sail Body-Fixed Hovering over Elongated Asteroids. Journal of Guidance Control and Dynamics 39 (6), 1223-1231, doi: 10.2514/1.G001061, 2016.

Zeng, X.Y., Jiang, F.H., Li, J.F. Asteroid body-fixed hovering using nonideal solar sails. Research in Astronomy and Astrophysics 15 (4), 597-607, doi: 10.1088/1674-4527/15/4/011, 2015.